



Experimental study on seismic upgrading of RC frames using innovative brace system with two-stage characteristic

Jianchen Zhao¹ · Jian Sun¹ · Hongxing Qiu¹

Received: 14 February 2022 / Revised: 12 April 2022 / Accepted: 14 April 2022 / Published online: 13 May 2022
© Wrocław University of Science and Technology 2022

Abstract

A novel gapped eccentric steel brace (GESB) was proposed to achieve a two-stage retrofit strategy for seismic upgrading of reinforced concrete (RC) frames. The steel brace was isolated from the RC frame at low story drifts using thin layers of polymer cellular materials, while the brace was activated at high drifts. Mild steel coupling beam was introduced into the brace system as a damper to improve the energy dissipation capacity of the system. Four frames were subjected to pseudo-static reversed cyclic loading procedure, including one bare frame and three retrofitted frames with the novel system. The experimental results indicated that the GESB system presented an obvious two-stage behavior which was generally superior in terms of providing second-stage enhancement of stiffness while avoiding drastic intervention in the initial vibration characteristics of the primary structure. Besides, the yield of mild steel beam greatly increased the energy dissipation capacity of the system. Compared with the reference frame, cracks were more diffuse in the retrofitted frames rather than concentrated at the column end, which means all of the original structure elements were fully used.

Keywords Cellular material · Mild steel damper · RC frame retrofitting · Eccentric steel brace · Two-stage characteristic

1 Introduction

It is important to improve the seismic performance of deficient existing RC frame buildings to reduce the economic losses and casualties caused by earthquake [1]. A number of retrofitting techniques have been adopted in past practice, including global retrofitting techniques, such as the addition of reinforced masonry [2] or concrete walls [3], external substructures [4], base isolation [5] and auxiliary energy dissipators [6], and local modification techniques [7], for instance, strengthening columns, beams and joints by concrete [8] or steel jackets [9] as well as fiber composite materials [10].

The selection of any of the technique depends on various technical, financial and sociological considerations [11]. Some global retrofit approaches without wet work (e.g.,

installing steel braces [12] or precast shear walls [13]) are considered more attractive due to short intervention downtime and low financial costs. In particular, eccentric steel brace systems are preferred for retrofitting RC frames with strong beam and weak column, benefit from the ability to reduce damage to the columns and provide strength and stiffness through taking advantage of beams [14].

However, improving stiffness often means the increase of seismic action in the retrofitted structure, which is very likely to aggravate the early structural damage for some specific structures. In addition, dramatic reductions in ductility of the retrofitted RC frame by steel brace system have been observed in both numerical [15] and experimental [16] studies. This is unescapable because the increased internal forces of these additional systems are eventually transmitted to the concrete frame, thereby accelerating local failure and reducing ductility. The consequence is even more serious for global structures, because the retrofitting increases the seismic action of the structure and thus accelerates the local failure, which may cause undesirable vertical irregular drift response.

A number of innovative brace systems with the intervention of damping have been proposed to mitigate structural seismic action, such as BRB [17], diagonal [18] or

✉ Jian Sun
sunjian@seu.edu.cn

Hongxing Qiu
qhxl01000854@163.com

¹ Key Laboratory of Concrete and Prestressed Concrete Structures of the Ministry of Education, Southeast University, Nanjing, Jiangsu, China

Y-braces with metal yield dampers [19] and friction dampers [20]. But these systems have low compensation ability for structural stiffness, hence may not be able to effectively prevent structural damage when large displacement demand is required. Therefore, more effective retrofitting strategies are necessary.

Another innovative retrofit strategy is aimed at providing second-stage enhancement of post-yielding stiffness of structure to serve as a safety reserve for large earthquakes while avoiding drastic intervention in the vibration characteristics of the primary structure, and reducing displacement demand on a global scale as a result [21]. Most recently, a numerical study [22] has disclosed the superiority of the retrofitting strategy with a two-stage characteristic that allows structures to represent particular behaviors at different stages. In the first stage, energy-dissipating devices can be introduced to weaken the vibration response of the structure, while in the second stage, the stiffness and strength of the structure are improved to compensate for the weakness of the damper and the degradation of the structural stiffness, thus preventing the collapse of the structure.

Several approaches have been proposed to try to match two-stage features. The introduction of special dampers with hardening-post-yielding stiffness [23] or multilevel yielding phases [24] could lift the structural strength under high displacement demands. But such an increase in stiffness and strength is insignificant for the global structure. The schemes with gapped characteristic were proposed to obtain a significant second-stage stiffness lifting of the structure, such as the steel bracing system with gap [25] and innovative gapped infills [26]. However, for common defective concrete frames, these techniques cannot inhibit structural damage in the first stage because the damping of the structure is not upgrade. In this case, more effective retrofit techniques should be developed.

In the present study, a new scheme is proposed to meet the two-stage retrofit strategy by introducing materials of different roles in an eccentric bracing system, called gapped eccentric steel brace (GESB) system. An isolation layer of

a highly deformable material with the capacity to absorb energy, namely a polymer cellular material, is placed at the supporting point interface between brace and frame, aiming at modifying the response of the retrofitted frame into a more favorable one for seismic actions. An energy dissipation device made by low yield point steel was introduced into the system to mitigate the seismic requirements of the structure.

2 The novel gapped eccentric steel brace system

Figure 1 illuminates the concept of the two-stage retrofitting strategy, illuminating that the system allows a partial retrofitting to the structure and has ability to provide a second stiffness lift to meet safety demand of the global structure, while minimizing the impact of the retrofit on the initial stiffness of the structure to avoid amplifying the seismic demand. In addition, the introduction of energy dissipation devices allows increasing damping in the first stage to further reduce the seismic demand. As shown in Fig. 1c, the retrofitted structure has a lower seismic demand under the design earthquake, which means less damage. In addition, the performance requirements under strong earthquake are satisfied due to the stiffness and strength lifting in the second stage.

The configuration of the GESB system is displayed in Fig. 2, illustrating the isolated frame and internal steel brace system. The frame and the brace are connected at the end of the diagonal strut (the clamping joint) by clamping the RC beam using two steel plates. The cellular material is installed to isolate the initial interaction of the beam and brace. This kind of fully assembled dry connection method avoids drilling holes and planting bars on the frame beam, so as to prevent the beam from corresponding damage. In addition, this connection is easy to achieve in practice by drilling holes on the floor slab. The initial horizontal component force of the diagonal brace is transferred to the bracket

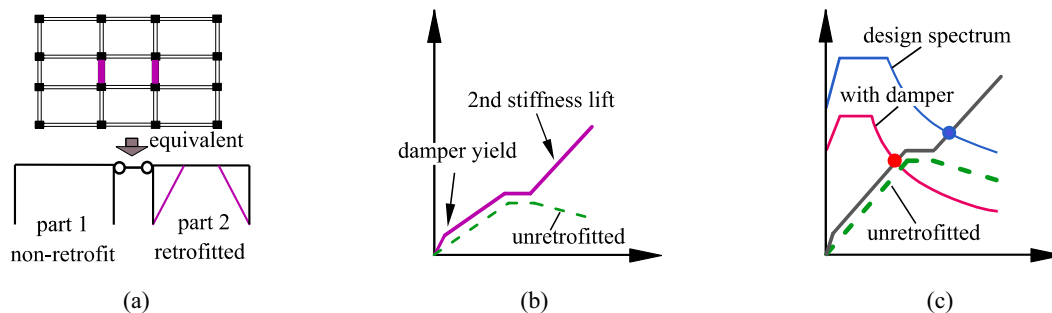


Fig. 1 The two-stage retrofitting concept: **a** partial retrofitting scheme; **b** capacity curve of part 1 (green dashed line) and part 2 (purple line); **c** global response

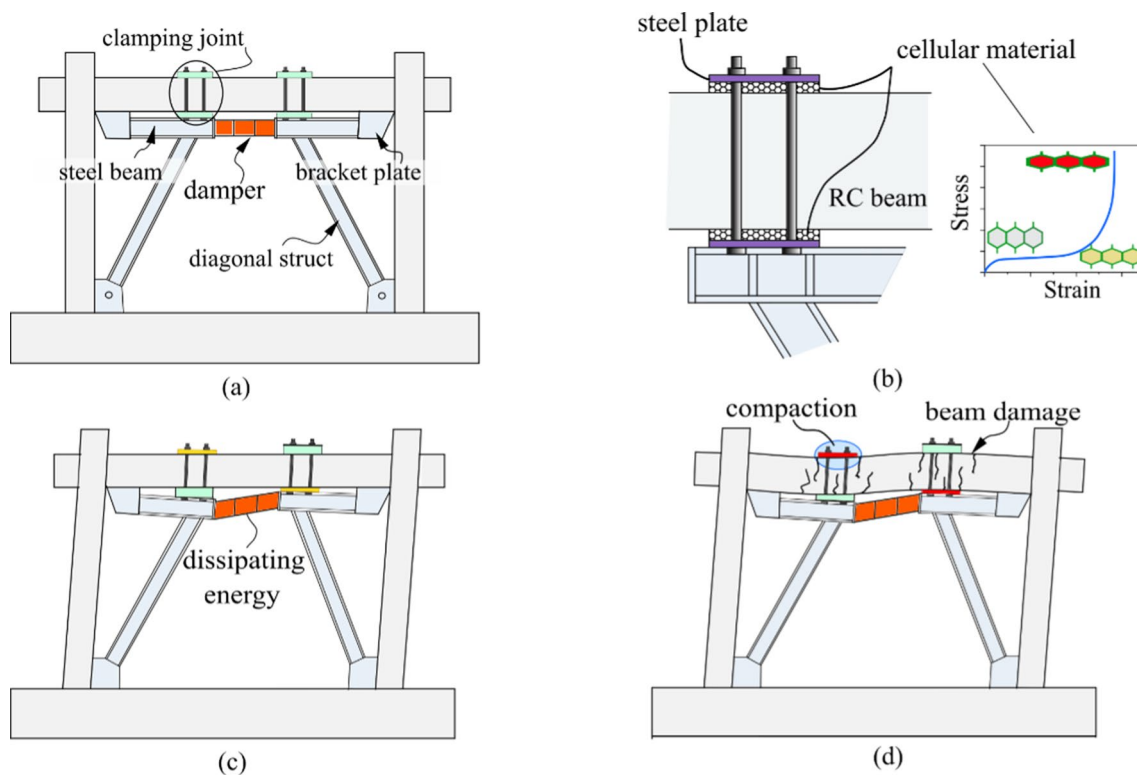


Fig. 2 Schematic illustration of the mechanism of GESB system: **a** elevation; **b** the clamping joint with cellular material; **c** the first-stage response; **d** the second-stage response

anchor plate fixed on the RC frame beam end through the steel beam to weaken the local shear failure of RC column caused by locally concentrated horizontal force. Adopted cellular materials have the capacity to develop extremely large strains in compression depending on their porosity and can effectively alleviate the vibration and shock produced by the earthquake. In previous studies, similar materials have been used as ideal elements for the isolation between infill walls and RC frames [26]. After reaching an adequate strain, the stress of the material increases dramatically, allowing the transferring of force between brace and frame.

Metal shear coupling beam made of mild steel material was introduced as a damper in the brace system. The adopted material has been proven to have an excellent damping effect because of its remarkable mechanical properties, including its specific low yield stress and excellent ductility [27].

The ideal response mechanism is provided in Fig. 2c, d. In the first stage, the brace and frame are isolated at small drift by the cellular material, and the system exhibits bare frame response with the damper operating to dissipate energy. As the drift increases, the cellular material is highly compressed and the steel brace is activated to compensate for the loss of horizontal and vertical capacity of the column resulting in the combination of brace and frame (called “compaction”), which provides additional strength and stiffness to

the structural system and constitutes the second stage of the response of the GESB system.

3 Experimental program

3.1 Description of test RC frames

To experimentally study the in-plane cyclic response of steel braced concrete frames with porous material joints isolated and mild steel energy dissipation coupling beam, quasi-static tests were carried out on 1/3 scaled single-layer and single-bay frames, extracting from the first story of an RC frame building, as shown in Fig. 3. The building was designed according to the Chinese Code GBJ11-1989 [28], representing typical architectural practices of existing structures in southwest China.

All linear geometric dimensions of the beam and columns as well as steel bars of test specimens were reduced by the scaling factor $SL = 1/3$. Figure 4a reports the 1:3 scale test frame model prepared for the quasi-static cycle test with details of beam/column sections. The column section was square with a size of 160 mm, and the beam section was rectangular with a size of 120 × 200 mm. The thickness of the cover concrete was 10 mm. The deformed

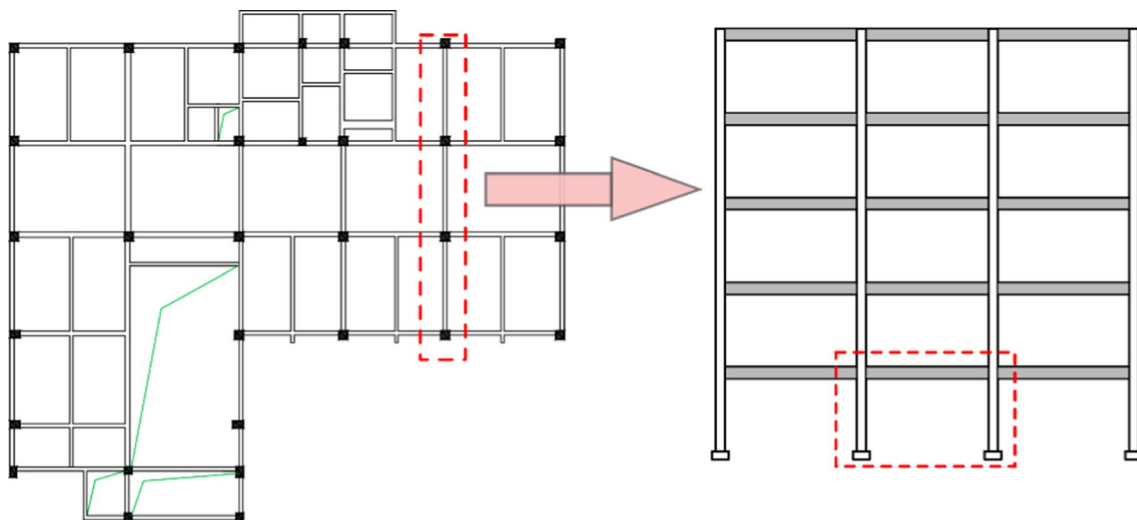


Fig. 3 Test RC frame in prototype structure

bars with a diameter of 10 mm and the plain bars with a diameter of 6 mm were adopted to constitute longitudinal and transverse reinforcement, respectively.

A total of four specimens were manufactured and then tested. In particular, BF represents the bare frame to provide a contrast. SP-1 and SP-2 are GESB retrofitted frames with/without damper. SP-3 adopts a large eccentricity to reveal the potential impact of different eccentricities on the performance of the system. Table 1 shows the configuration of test specimens.

For the shear coupling beam damper, the relative length ratio is usually required to meet the following equation to ensure the shear yield mechanism [29].

$$e/(M_{lp}/V_{lp}) < 1.6, \tag{1}$$

where e is the effective length of the energy dissipation beam; M_{lp} , V_{lp} the plastic flexural and plastic shear capacities of the beam, respectively, which can be calculated by the following formulas:

$$M_{lp} = f_y Z, \tag{2}$$

$$V_{lp} = f_v A_w = \frac{f_v}{\sqrt{3}} A_w, \tag{3}$$

where f_y and f_v the tensile and shear yield strength of steel, respectively; A_w the measured cross-sectional area of the shear web; Z the plastic section modulus.

The dimension of the shear beam is shown in Fig. 5. According to the calculation, the relative length ratio is 0.77, meaning that it is a short energy-dissipating beam segment, and the effective plastic angle could exceed 0.15 rad [30].

Ribbed stiffeners were welded in compliance with the limit distance requirements of AISC 341-10 [31] and GB 50011-2010 [32]. Moreover, the stiffeners were chamfered to prevent additional damage at the web and flange joints induced by stiffeners welding, as shown in Fig. 5.

In this test, the bracing buckling is not expected. Hence, sufficient sectional size is adopted, which means the bracing remains elastic during the loading (Fig. 6).

Before “compaction” occurs, the brace only bears the force transmitted by the deformation of the steel coupling beam. After “compaction”, the bracing is integrated with the reinforced concrete frame, and the axial force of the diagonal bracing P can be divided into two parts: the force transmitted by the coupling beam (P_d) and the force generated by clamping of RC beam and brace (P_{df}).

$$P = P_d + P_{df} = \frac{V_{Lu} \cdot L}{2H \cos \theta} + \frac{V_{Lu,RC} \cdot L}{2H \cos \theta}, \tag{4}$$

where V_{Lu} is the shear limit of the steel coupling beam, and $V_{Lu,RC}$ is the shear limit of the RC beam.

$$V_{Lu} = \min \{2M_{lp}/e, V_{lp}\} \cdot \Omega, \tag{5}$$

$$V_{Lu,RC} = \min \{2M_u/e, V_u\}. \tag{6}$$

Ω is the overstrength ratio, which is set to 1.5 according to AISC standard [29]. M_u and V_u are the flexural and shear strength of RC beam according to the actual reinforcement.

Similarly, the axial force of a steel beam can be derived as:

$$N = N_L + N_{Lf} = P \cos \theta. \tag{7}$$

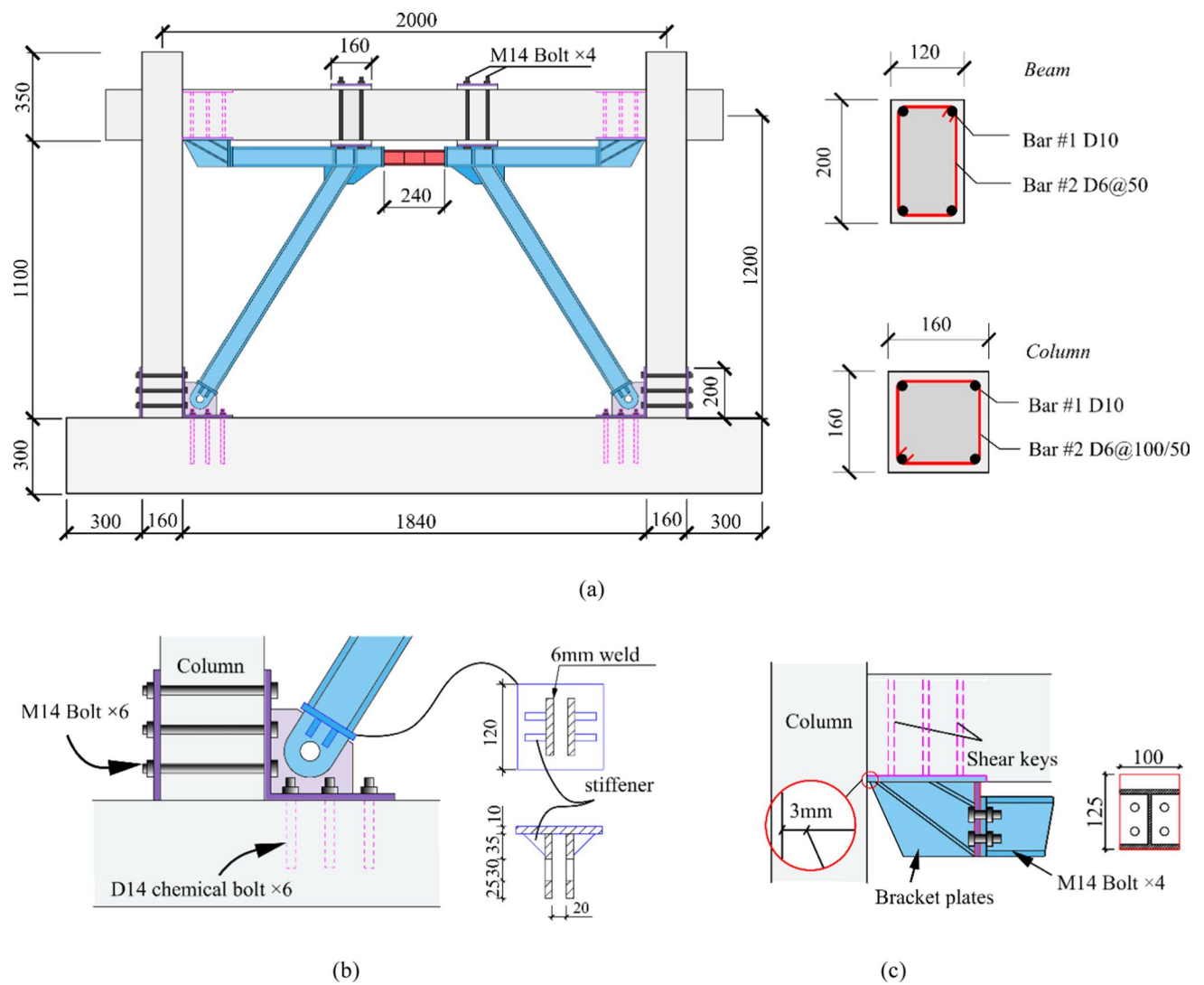


Fig. 4 Test frame details: **a** Elevation and sections of beam and column; **b** the hinged shoe of the diagonal strut; **c** the bracket anchor plates of the steel beam (unit: mm)

Table 1 Configuration of test specimens

specimen	Retrofit type	Cellular material thickness (mm)	Eccentric (mm)	damper
BF	Bare Frame			
SP-1	Short GESB	7.5	500	None
SP-2	Short GESB	7.5	500	BL160 coupling beam
SP-3	Long GESB	6.5	700	BL160 coupling beam

On the premise of meeting the above calculation requirements and taking into account the convenience of materials, the brace in this test was made of 100*100H beam steel, and the material is Q235 steel.

At each clamping joint, the brace was connected to the frame beam by four 14 mm bolts. Bolts and chemical anchors were used to connect the hinge points to the frame

as shown in Fig. 4b. The bracket anchor plates of the steel beam were planted in RC beam with six 14 mm bolts used as shear keys as shown in Fig. 4c, which met the requirements of GB50010 [33].

According to the proposed retrofit strategy, the ‘‘compaction’’ of brace and RC frame should provide additional stiffness and strength when the strength of the RC frame

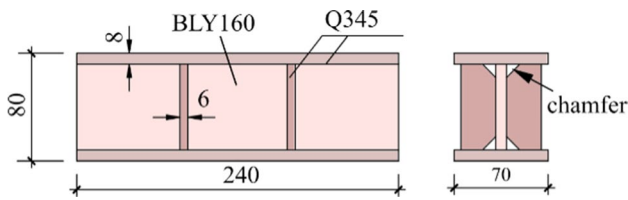


Fig. 5 The dimension of the shear beam (unit: mm)

deteriorates. Therefore, the drift demand of “compaction” should be greater than the yield displacement point of the frame.

The thickness of the cellular material isolation layer determines the displacement requirements for the “compaction” of brace and frame (Fig. 7).

The vertical displacement at the clamping joint point is:

$$\Delta_d = \frac{a}{H} \cdot \Delta_c \tag{8}$$

Considering that the plastic hinge first appears in the column at the beam–column joints of the existing weak RC frame while the beam ends remain elastic, it is acceptable to ignore the deformation of the RC beam caused by horizontal loads in the primary design procedure.

Assuming that the “compaction” occurs when the drift ratio is γ_1 , the thickness of the cellular material is:

$$s = \Delta_d / \eta = a\gamma_1 / \eta, \tag{9}$$

η is the compaction strain of the material, which can be obtained from the monotonic compression test results.

RC frames usually yield at the interlayer drift ratio of about 0.5–1% [34]. In addition, to reflect the change of displacement–load curve more clearly before and after “compaction” and to reduce the influence of construction error, the drift ratio demand in this test is set at 1%. This consideration is acceptable since the test focuses on

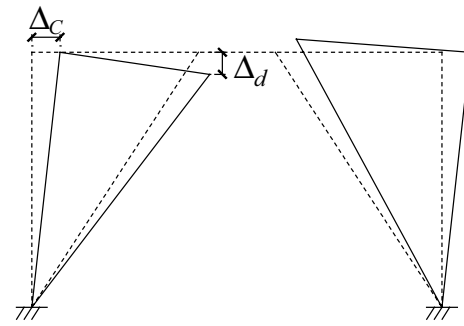


Fig. 7 The deformation of internal steel brace

verifying the feasibility of the present retrofit strategy. The thickness of the cellular material in SP-1 and SP-2 was 7.5 mm, and that in SP-3 was 6.5 mm, representing 1% of the drift ratio demand.

3.2 Material properties

All of the RC frames were cast in one batch. Six standard concrete cubes with sizes of 150 mm were also prepared for compression test following GB/T 50081 [35]. The measured average compressive strength of the cubes was 32.13 MPa meaning the prismatic compressive strength was equal to 21.49 MPa with a reduction factor of 0.76 according to GB/T 50152 [36].

In the present study, the web of the shear damper is made of LY160 mild steel, while the flange and stiffener are made of high strength steel Q345. The tension test was carried out on steel sample for each type of reinforcement bars and steel plates according to GB/T 228.1 [37], with the measured material properties summarized in Table 2.

The polymer cellular material adopted in this test is (Ethylene Vinyl Acetate) EVA composite foaming material made by moulding forming method, with azodicarbonamide (AC) as foaming agent and bis

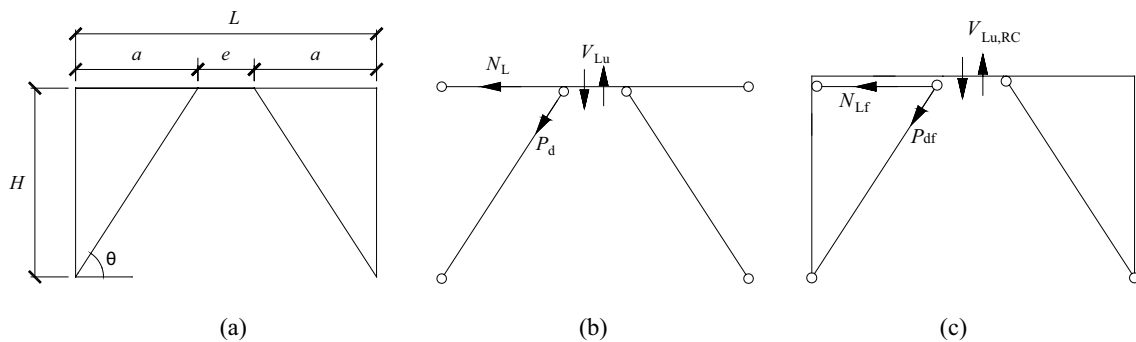


Fig. 6 Mechanical schematic of steel brace system **a** dimension, **b** internal steel brace before brace activation, **c** brace–frame system with porous material compacted

(1-(Tert-Butylperoxy)-1-methylethyl)-benzene (BIPB) as cross-linking agent. This closed cell foam material has independent pore structure due to the wall film between the internal bubble holes, and play a prominent role in high strength impact resistance, shock absorption, vibration reduction, noise reduction, and heat insulation functions. Key parameters of the material are shown in Table 3.

The monotonic compression test of the porous material was carried out according to GB/T 18942.1 [38] to obtain the characteristics of the isolation layer. Three groups of cuboid samples with side length of 20 mm and thickness of 10 mm were prepared from the original materials. The compression speed was set to 30 mm/min, 24 mm/min and 12 mm/min, respectively, and the test was stopped when

the stress increased sharply and the specimen was fully compacted.

As can be seen from Fig. 8a, the stress–strain curves of the material are slightly different under different loading speeds, and the curves are basically the same at large strains, which indicates that the loading speed has negligible effect on the mechanical properties. Figure 8b shows the mean value of stress under the three loading speeds. The ordinate is extended to a larger scale to depict the global stress–strain response. It can be seen that the stress increases sharply when the strain exceeds 0.9, which suggests that the porous material has been completely compressed and can effectively transfer the load.

Table 2 Measured material properties

Material	Measured dimensions (mm)		Yield strength (MPa)	Ultimate strength (MPa)	Location
	Diameter	Thickness			
Steel bar #1	9.98		452.38	549.46	Longitudinal bar
Steel bar #2	6.12		377.12	495.4	Stirrups
H-shaped steel		7.91	298.43	392.51	Internal brace
Q345		7.98	357.37	435.61	Flange of coupling beam
LY160		7.64	151.39	275.09	Web of coupling beam
M14 Bolt	14.12		759.05	864.84	Clamping point

Table 3 Parameters of the adopted EVA cellular material

Apparent density (kg/m ³)	Pore density (number /m ³)	Pore diameter (μm)	Shore hardness	Tear strength (kN/m)	Resilience rate (%)	Permanent compression set (%)
201	6.1×10^{13}	51.2	40	8.9	43	15

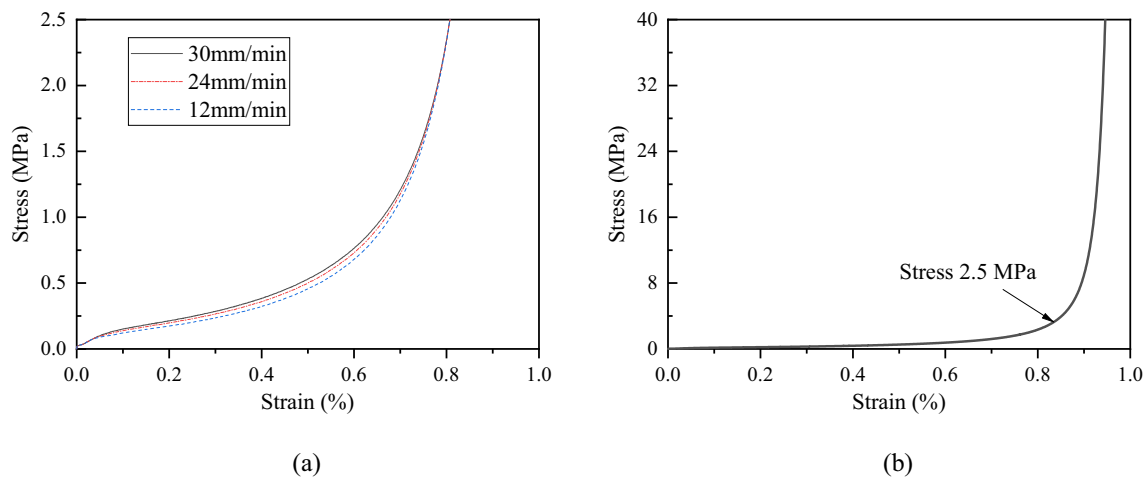


Fig. 8 Compressive stress–strain curve of the cellular material: **a** stress–strain curves with different loading speeds; **b** mean stress value under different loading speeds

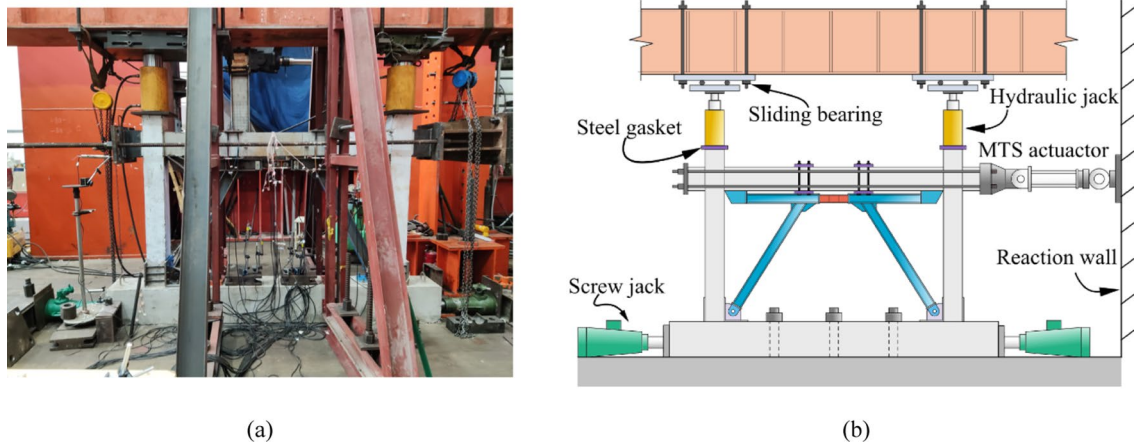


Fig. 9 Testing set-up: **a** Photo; **b** Schematic

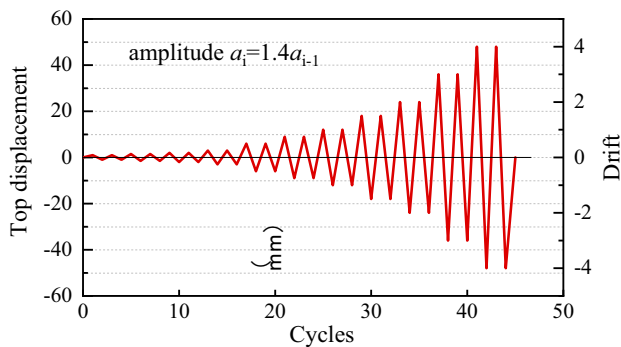


Fig. 10 Loading protocol

3.3 Experimental set-up and procedure

A general view of the experimental set-up and instrumentation is shown in Fig. 9. The strong foundation beam was fixed to the floor via three prestressing rods to provide full clamping. All frame columns were suffered from axial force with a value of 150 kN (represent an axial load ratio of 0.2) through hydraulic jacks seated above every column to simulate gravity load. The sliding support is introduced under the reaction frame so that the jack can move with the frame column. The horizontal load was applied directly on the rigid area of the frame beam end using an MTS actuator. Gravity loads on the concrete beams were not taken into account, which was the same as some other experiments on bracing systems [14, 16], considering that the effect of the gravity load is very small compared with the seismic action of the frame. On the other hand, the beam–column joint area is protected due to the “compaction” of the system, so the shear force generated by the gravity loads is difficult to cause an obvious negative effect on the structure. In this regard, the results obtained by the present experiment are acceptable.

Deformation-controlled loading was adopted in the test. The loading amplitude and the number of cycles were determined in accordance with FEMA461 [39], as described in Fig. 10. The drift was defined as the ratio of horizontal displacement to frame height (1.2 m) was measured from the lateral loading point to the top surface of the foundation block.

4 Experimental results

4.1 Observed damage mechanism of tested frames

4.1.1 Specimen of BF

Initial flexure cracks were observed at the toe and top of columns during the load step running to 2 mm (0.17% drift ratio) and 2.5 mm (0.21% drift ratio), respectively. With the increase of loading step, new cracks appeared constantly and the existing cracks widened, extended further and intersected gradually. Cover spalling was observed at the toe of columns when the load step running to 9 mm (0.75% drift ratio) and the flexure cracks at the top of columns widened further. Slight flexure cracks appeared at the beam when the load step running to 12 mm (1% drift ratio). Cracks in the column top began to develop to the edge of the beam–column joint under this run.

Slight shear cracks appeared in the joint during the load step running to 18 mm (1.5% drift ratio). Cover spalling was observed at the top of columns when loading to 24 mm (2% drift ratio) and the flexure cracks at two sides of the frame beam end intersected.

Finally, when the value of loading displacement of 48 mm (4% drift ratio) was achieved, concrete cover spalling was observed at joints margin with the joint shear cracks widening (Fig. 11a), and concrete crumbled off at the bottom

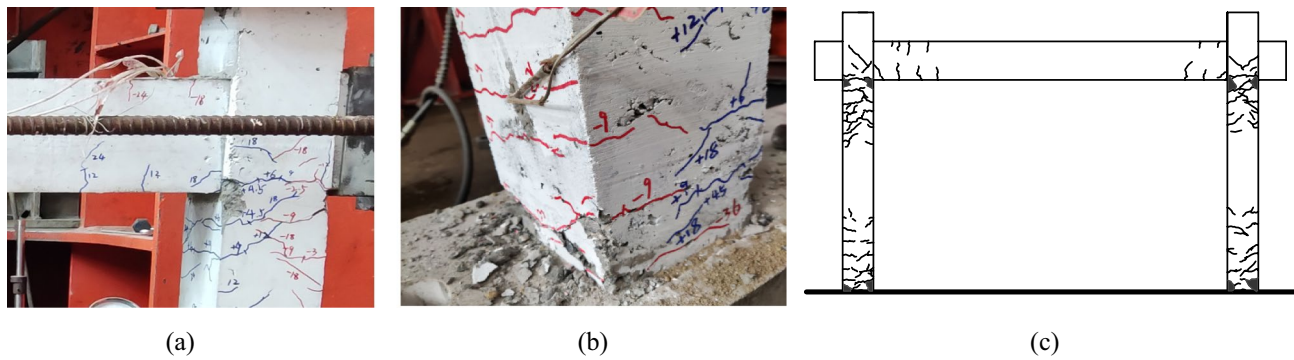


Fig. 11 Damage observation in BF: **a** joint shear cracks; **b** concrete crumbled at the column bottom; **c** global cracks pattern

corner of the column as shown in Fig. 11b. However, few new cracks were observed at the beam ends.

4.1.2 Specimen of SP-1

SP-1 was retrofitted by GESB without damper. Initial flexure cracks were observed at the toe and top of columns when the load step running to 2 mm (0.17% drift ratio) and 2.5 mm (0.21% drift ratio), respectively. The development of cracks was similar to that of BF until flexure cracks appeared in the plastic hinge area of RC beam when the load step running to 9 mm (0.75% drift ratio), which expanded away from the beam ends under subsequent runs. The cellular material at the clamping joints was found to be squeezed when loading to 12 mm (1% drift ratio), after which cracks in column tops and beam ends had almost stopped growing. Flexure cracks were observed at the clamping joints of the frame beam and developed to both sides of the joints when loading to 18 mm (1.5% drift ratio). Slight shear cracks appeared between the two clamping joints (eccentricity segment) when loading to 24 mm (2% drift ratio), and increased continuously with increasing load. When the loading displacement reached 48 mm, concrete crumbled off at the bottom corner of

the column (Fig. 12a), and the width of shear cracks at the eccentricity segment had increased significantly with concrete spalling and crushing. Wide flexure cracks were observed at the clamping joints of the beam as shown in Fig. 12b. The frame beam was broken by coupling of shear failure at eccentricity segment and flexure failure at clamping joints due to the “compaction” of brace and frame as shown in Fig. 12c.

4.1.3 Specimen of SP-2

SP-2 was equipped with a mild steel shear coupling beam in the brace. Flexural cracks also appeared first at the toe of columns when the load step running to 2 mm (0.17% drift ratio). Several horizontal cracks were observed at the top of columns when loading to 4.5 mm (0.38% drift ratio). Slight flexure cracks initiated at the beam end under the top displacement of 6 mm (0.5% drift ratio). New beam cracks developed towards the brace-frame clamping joint, and were evenly distributed along the frame beam. Similar to SP-1, flexure cracks were observed at the clamping joints of the frame beam when loading to 18 mm (1.5% drift ratio), while few new cracks were found at the top of the column and the

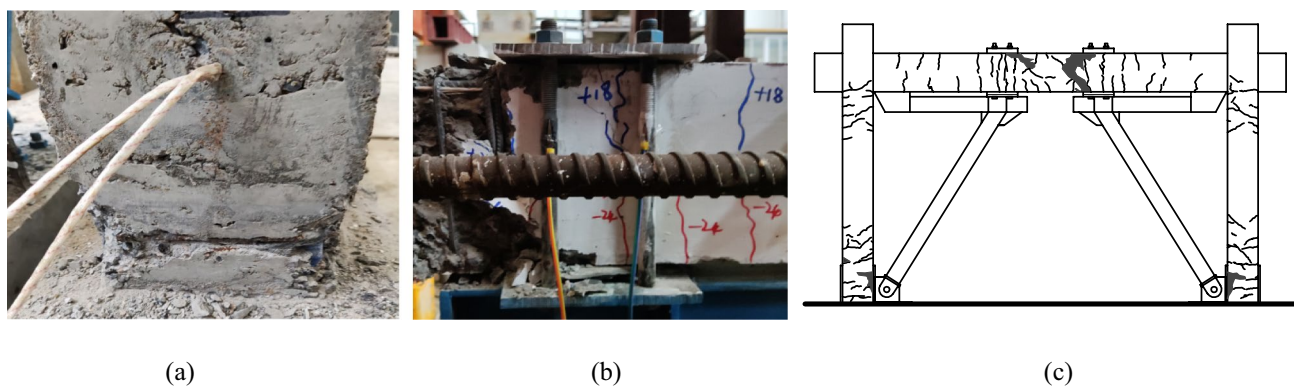


Fig. 12 Damage observation in SP-1: **a** concrete crumbled at the column bottom; **b** joint shear cracks; **c** global cracks pattern

end of the beam. As the load step running to 2% drift ratio, shear cracks initially occurred at the eccentricity segment, and the energy dissipation coupling beam had shown significant visible shear deformation. Welding cracks appeared at the end of the steel coupling beam at the loading displacement of 36 mm (3% drift ratio), and shear cracks at the eccentricity segment widened. When the loading displacement reached a value of 48 mm (4% drift ratio), the steel coupling beam was acutely damaged due to weld fracture (Fig. 13b). The structure was considered failed due to the piercing wide flexure cracks and the splitting concrete at the clamping joints as well as the remarkable shear cracks at the eccentricity segment as depicted in Fig. 13c.

4.1.4 Specimen of SP-3

SP-3 had a longer eccentricity segment of the frame beam than SP-2. SP-3 had a comparable behavior to SP-2 under low displacement ratio load step, with initial cracks discovered at the base and top of columns during the load step

running to 2 mm and 4.5 mm, respectively. When loading to 6 mm (0.5% drift ratio), several slight cracks were observed at the beam end and gradually developed to the brace-frame clamping joint under subsequent test runs. Cacks on the beam distributed over a length of 500 mm away from the beam end under story displacement of 9 mm (0.75% drift ratio). Flexure cracks with 1 mm width were observed at the clamping joints of the frame beam under the top displacement of 18 mm (1.5% drift ratio), while almost no new crack in column tops or beam ends was observed during this run. Weld cracks were observed at the end of the coupling beam and solder joints were detached on the top surface of the beam when the load step running to 3% drift ratio. When the loading displacement reached 48 mm, the flexure cracks at the clamping joints widened, and the concrete cover under the steel plate started spalling and crushing. After removing the steel plate, penetrating cracks were observed on the upper of the beam (Fig. 14a). However, shear failure was not discovered at the eccentricity segment of the RC beam as shown in Fig. 14b.

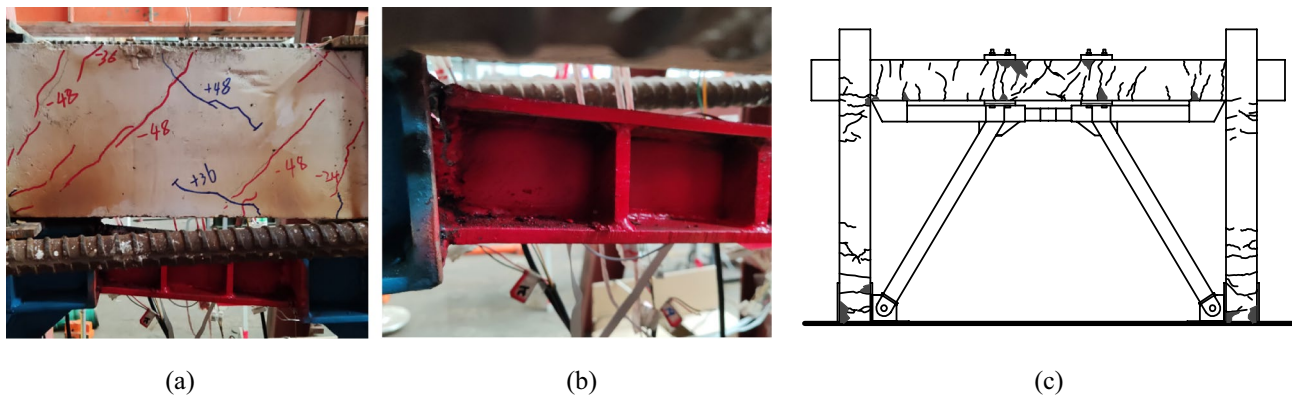


Fig. 13 Damage observation in SP-2: **a** shear cracks at the eccentricity segment; **b** weld fracture in the steel coupling beam; **c** global cracks pattern

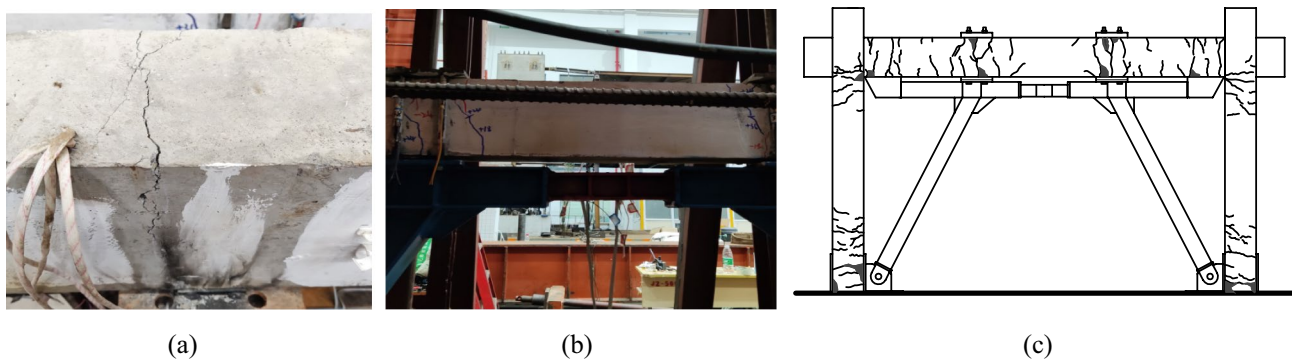


Fig. 14 Damage observation in SP-3: **a** penetrating cracks at the upper of the beam; **b** few shear cracks at the eccentricity segment; **c** global cracks pattern

4.1.5 Comparison of the test frames

Ascribe to the weak reinforcement configuration of the column, the failure mode of the frame is “strong beam–weak column”. The predominant damage showed a flexure hinging mechanism of columns at both top and bottom ends, which was followed by cover spalling at the base of columns. On the contrary, only a few cracks on the beam are concentrated in the plastic hinge area. The damage of the column is much greater than that of the frame beam.

The damage modes of retrofitted frames and BF developed in a similar way before the “compaction” occurred. Although the retrofit scheme allows the development of column hinging, the column end damage was restrained after the occurrence of “compaction”, while the beam damage was aggravated in the area of clamping joints, which demonstrated that all components in the retrofitted RC frame were fully utilized in deferent stage and played a full part in resisting load and consuming energy. Compared with BF, there are significantly more cracks appeared in RC frame beam in the retrofitted frames. And the cracks were not limited to the area of plastic hinges at the beam ends but presented a uniform and wide distribution.

Moreover, the retrofitted frame ultimately failed due to the failure of the RC beam rather than column hinging or joint cracking, meaning that retrofitting prevented structural collapse by avoiding severe column hinges. In particular, the frame beam of SP-1 and SP-2 suffered flexure and shear damage while the frame beam of SP-3 only presented flexure failure. Shear cracks were not observed at the eccentricity segment in SP-3, which could be attributed to the long eccentricity of this retrofitted specimen.

4.2 Load–displacement response

Figure 15 demonstrates the load–displacement behavior of the four frames. And the backbone curves are compared in Fig. 16.

The response of BF exhibited a ductility behavior with low strength. The peak strength of BF (occurred at a drift ratio of 1.97%) was 50.58 kN. Pinching effect was also observed, which could be ascribed to the flexure hinging of columns and shear cracking of column–beam joints.

The response of SP-1 showed a second ascending branch after the drift of “compaction” which was elucidated by black dash. The peak strength was equal to 192.58kN (occurred at a drift ratio of 2.98%), which was approximate 3.84 times the peak strength of BF. A slight increase of 7.7% was observed in the initial stiffness of the frame which indicated the retrofitting had little intervention on the stiffness. The hysteresis behavior presented a characteristic of reverse S-shape due to the affect caused by the gap.

The hysteresis loops of SP-2 and SP-3 were notably wider than those of SP-1 due to the significant energy dissipation ability of the mild steel beam in the brace, which yielded before the RC frame and dissipated energy through plastic deformation. Because of the isotropic strengthening phenomenon of the mild steel, the hysteresis loop was continuously expanding under early load steps. After the ratio reaches about 3%, the hysteresis loop area decreases with the strength provided by the coupling beam almost completely disappearing due to failure of the beam. However, the strength was not reduced to the level of BF, demonstrating the frame still had a relatively high ability to resist load due to the effect of “compaction”. This means the brace provided subsequent security for the retrofitted system and could prevent the structure from collapsing.

Ascribe to the longer eccentricity, the “compaction” phenomenon of SP-3 was more moderate than that of SP-2 manifested by a lower raising strength in the second ascending branch. However, attributed to the shear failure of the RC frame beam in SP-2, the strength of SP-2 decreased more significantly than that of SP-3 at a drift ratio of 4% even though both of them experienced the same strength loss caused by damper failure after a drift ratio of 3%.

On the other hand, significant increases in initial stiffness of SP-2 and SP-3 were observed. Note that this kind of increased stiffness was derived from the contribution of the damper, and would not induce an increase in seismic demand of structures. In contrast, the structural seismic demand could be suppressed because of the damping effect provided by the early yield of the dampers.

4.3 Measured strain in reinforcing bars

Figure 17a shows the inconspicuous differences in the strains of the vertical steel bars at the bottom of the column for different frames. The reason is that the top displacement of single-bay frame was positively correlated with the chord rotation at the toe of column which was directly related to the strain of the bottom steel bars. However, the brace system changed the internal force distribution of the structure after “compaction” drift (represented by the black dash), hence reduced the bending moment and shear action of the frame column and affected the deformation mode of the column [40], finally led to a slightly lower reinforcement strain demand at the bottom column of the retrofitted frame than BF.

Due to the yield mechanism of the column hinge, the strain of the vertical steel bars at the column top grew signally with loading drift increasing and reached the yield strain at the displacement of about 6 mm as depicted in Fig. 17b. The strain results of the retrofitted frames were suppressed after the “compaction” drift, indicating that this mechanism restricted the further development of the damage

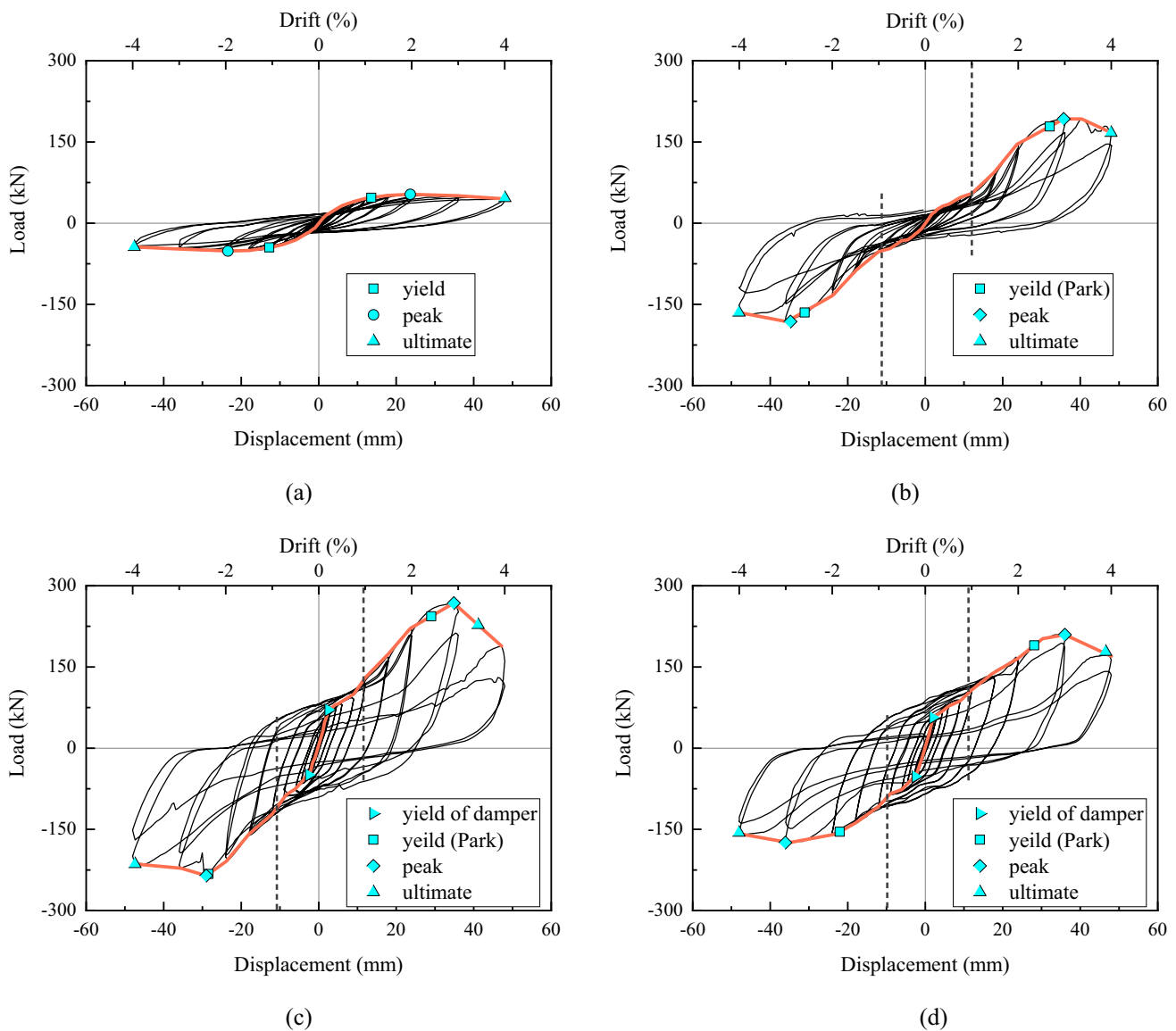


Fig. 15 Measured load-top displacement responses: **a** BF; **b** SP-1; **c** SP-2; **d** SP-3

in column top, which was corresponding to the experimental phenomenon.

The strains measured in the longitudinal bars at frame beams end are reported in Fig. 17c, with the strain in the beam-end bars of BF being significantly lower than those of retrofitted frames and not reaching yield strain. This was also ascribed to the column hinge yield mechanism of the frame. After the yield of the reinforcements at the top of the column, the deformation was significantly concentrated at the end of the weak column rather than the beam, hence the chord rotation demand of the beam end was reduced. In the retrofitted frame, the eccentric axial force provided by the steel beam of the brace increased the bending moment at the RC beam end, resulting in the

increase of the strain measured in the longitudinal bars. On the other hand, the strain of the reinforcing bars at beam end was restricted to develop with drift ratio increasing. In fact, the "compaction" mechanism suppressed the chord rotation demand of the beam end and inhibited the continuous rise of the reinforcing bars strain as a result.

Figure 17d shows the measured reinforcing bars strains at the clamping joint of the RC beams in the retrofitted frames. After the "compaction" drift ratio, a sudden elevation of reinforcement strain was observed, showing a remarkable two-stage characteristic. And the reinforcement yielded rapidly with the displacement increasing, indicating that the frame beam was damaged and participated in dissipating energy.

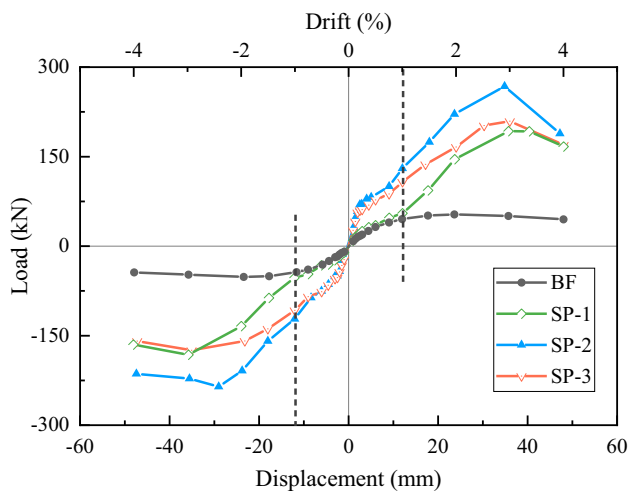


Fig. 16 Backbone curves

4.4 Measured strain in steel brace system

The measured axial strains of the bolts at the clamping joints and the strains of the diagonal struts in the steel brace system are reported in Fig. 18. The bolts strains of all frames exhibited a similar trend, with the strain value almost being zero at the beginning and presenting a sudden elevation after the drift of "compaction", which clearly demonstrated the two-stage characteristic of GESB system. After the RC beam yielded, the force tended to be stable, and the strain stopped growing with the increase of displacement. The same phenomenon could be also observed in measured strain results of the diagonal strut for SP-1 in Fig. 18b. Different from SP-1, the diagonal strut strain of SP-2 or SP-3 showed a larger value at the beginning attributed to the contribution of the coupling beam in the steel brace system. It can be also found that the slope of the strain decreased with the yielding of the damper, and increased again after the occurrence of "compaction".

5 Analysis of the test results

5.1 Stiffness reduction

The secant stiffness represents the slope of the line between the origin and maximum load of the first cycle in each loading stage [36], which is exhibited in Fig. 19. The secant stiffness degradation of SP-1 and BF was comparable before the drift of "compaction". However, the secant stiffness of SP-1 was found ascending after the occurrence of "compaction", indicating that brace system provided significant second-stage stiffness and slowed down the stiffness degradation.

The initial stiffness of SP-2 and SP-3 was larger and fell rapidly due to the contribution of the steel coupling beam. After the occurrence of "compaction", the degradation was also effectively slowed down, representing a compensation for the deterioration of the damper.

5.2 Drift capacity and ductility

Several points related to ductile behavior were summarized in Table 4. The drift capacity of BF was greater than that of the retrofitted frames (BF even had not reached the failure at 4% drift ratio in positive load direction), which was inevitable because the brace accelerated the failure of the frame beam as discussed previously. However, compared with traditional brace systems [14, 16], GESB is still attractive because that the initial isolated interaction between brace and beam delayed the onset of degradation of the retrofitted frame. Due to the larger eccentricity, the drift capacity of SP-3 increased by 11% (positive direction) than SP-2.

The displacement ductility ratio is considered as another indicator to evaluate the seismic performance of structures. It should be noted that the retrofitted frames exhibited obvious secondary ascending branches, which influences the traditional interpretation of yield point derived by Park method [41] (as shown in Fig. 15) as well as displacement ductility ratio. In this regard, the ductility ratio based on yield of reinforcement was considered as a supplement, which demonstrates similar ductility values between the retrofitted frames and BF.

The ductility of SP-3 is superior to that of SP-2 with the consideration of the results derived from whether park method or yield point of reinforcement. In view of the effect on drift capacity, the eccentric length of RC beam is an important factor which is related to the occurrence of shear failure and influence the ductility of the retrofitted frame. Consequently, a limited eccentricity ratio should be considered in retrofitting design procedure.

5.3 Energy dissipation

The equivalent viscous damping ratio and cumulative hysteretic energy are two common criteria to evaluate the energy dissipation capacity of structures [43]. As shown in Fig. 20, the equivalent viscous damping ratio of SP-1 reduced when "compaction" occurred due to the enhancement of stiffness and strength, and gradually increased with the drift increasing benefitted from energy dissipation effect produced by yielding of beam steel bars.

The equivalent damping ratio of SP-2 and SP-3 was significantly higher benefitted from the contribution of the mild steel coupling beam, and increased with the yielding and stress strengthening of the mild steel web, but also decreased with the occurrence of "compaction".

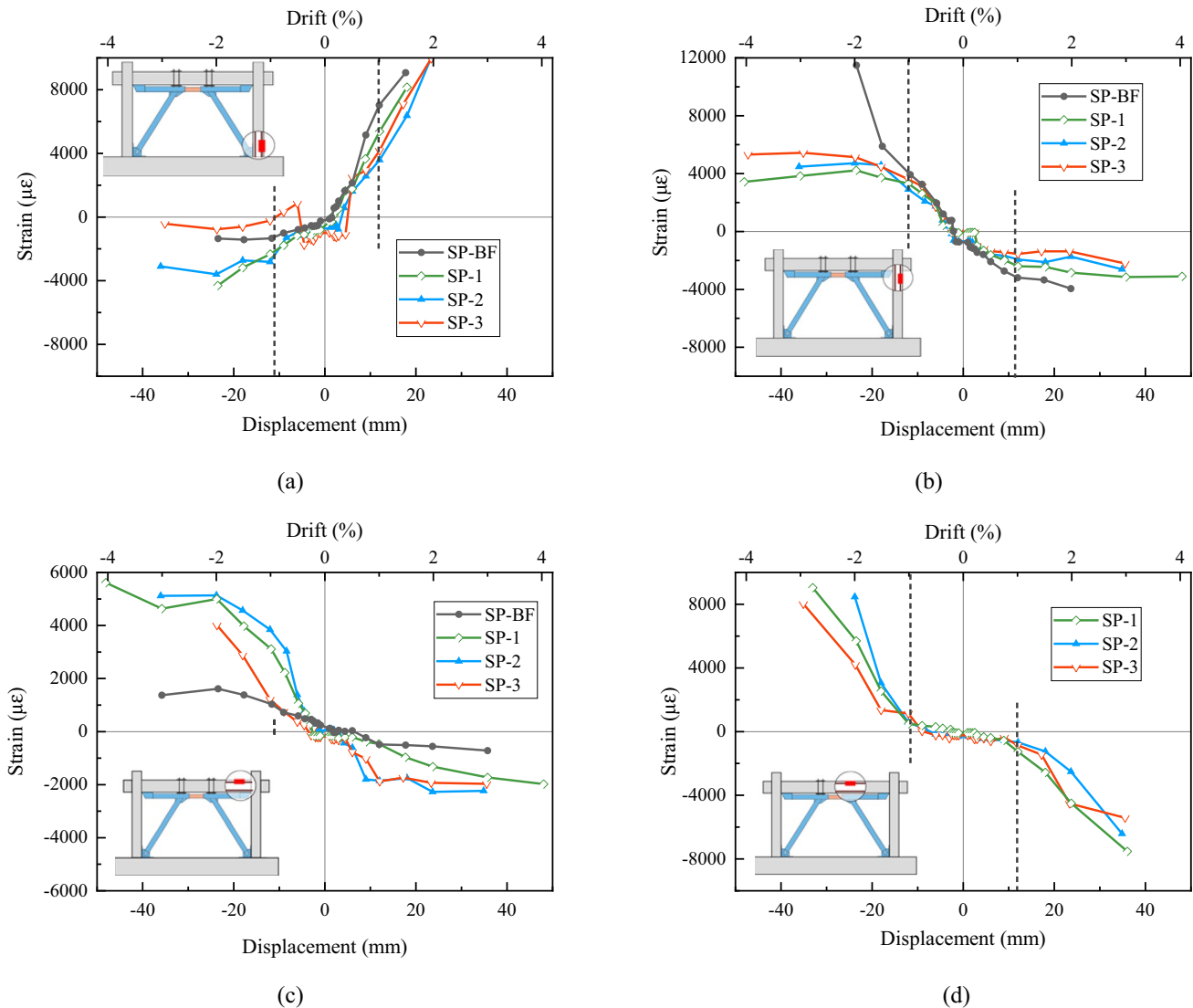


Fig. 17 Comparison of the strain results: **a** vertical bars at the toe of the column; **b** vertical bars at the top of the column; **c** longitudinal bars at the RC beam end; **d** longitudinal bars at clamping joint of the RC beam

When the load drift increased to about 3%, the energy dissipation capacity of the structure was rapidly weakened ascribed to the damage of the damper. The equivalent damping ratio of SP-2 was less than that of SP-3, because of the larger extra strength provided by "compaction". Moreover, the energy dissipation capacity was also suppressed due to the shear cracking of the eccentric segment in SP-2 frame beam.

In light of cumulative hysteretic energy, any retrofitted frame dissipated more energy than the bare frame. The results of the retrofitted frames with damper are more outstanding, which exhibited the ability to consume about 5 times as much energy as a bare frame.

6 Conclusions

Four RC frames were tested in the present research, including one bare frame and three retrofitted frames through the novel GESB system, which introduced cellular material to weaken the initial contact between the brace and the frame, with the mild steel coupling beam being adopted as a damper to improve the energy dissipation capacity of the system. All frames were subjected to pseudo-static reversed cyclic loading procedure with axial force applying on the column. Based on the experimental results, the following conclusions can be drawn.

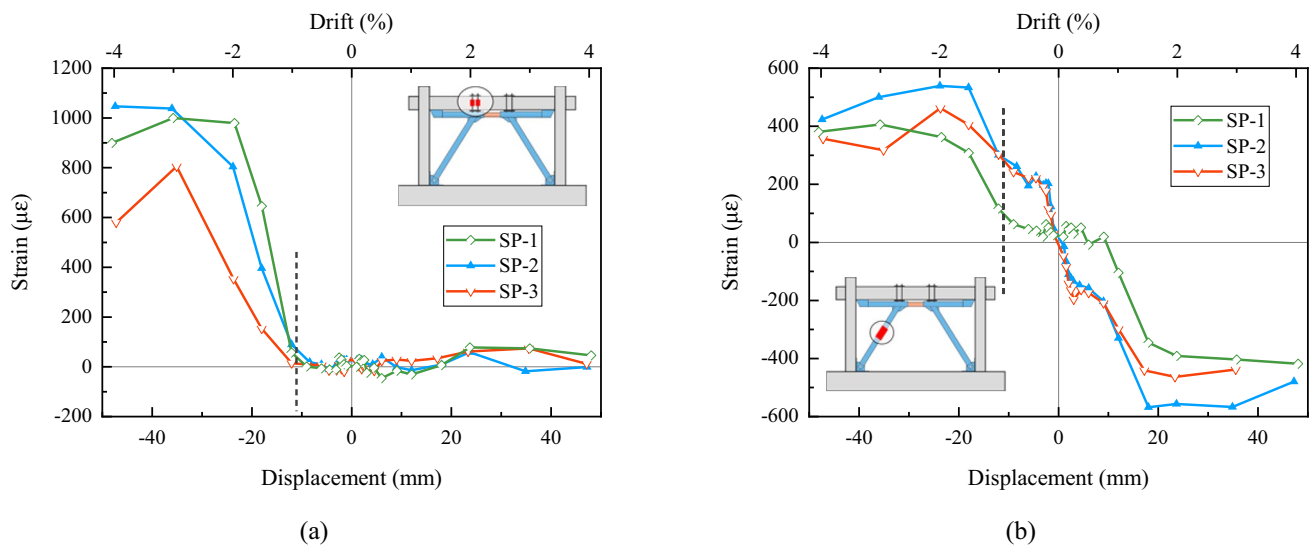


Fig. 18 Measured strain in brace system: **a** strains of reinforcing bolts at clamping joint; **b** strains of the inclined strut

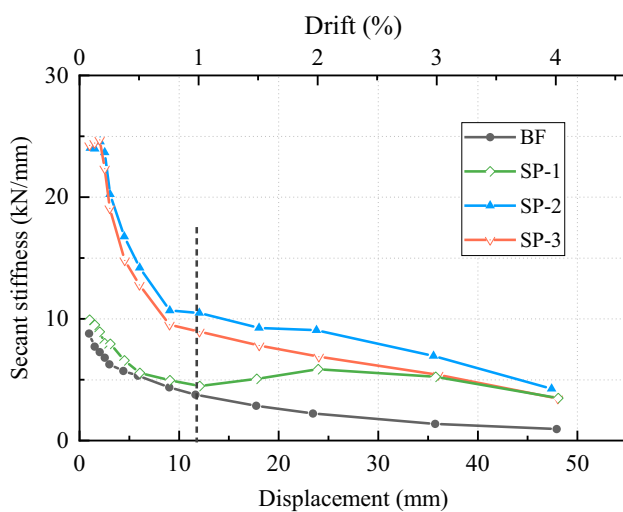


Fig. 19 Stiffness degradation

1. The isolation joints made of cellular materials can eliminate the frame–brace interaction (bare frame behavior) under small drifts. The initial stiffness of SP-1 was increased by only 7% compared to BF. However, as drift become large, the brace is activated with the cellular materials being fully compressed, thereby increasing the strength and stiffness of the frame–brace system, which shows an obvious two-stage characteristic. The peak strength of SP-1 was 192.58kN, which was approximate 3.84 times the peak strength of BF. The frame retrofitted with the GESB system exhibits bare frame behavior before "compaction" occurs, avoiding the improvement of the initial stiffness, that is, the seismic demand of the structure.
2. The GESB system inhibits sustained damage to the column after a certain amount of damage has occurred, and aggravates the damage to the frame beam compared with

Table 4 Summary of test results

Test frame	Loading direction	Yield point		Yield of steel bars		Failure point		μ_{park}	μ_s
		δ_y (%)	P_y (kN)	δ_s (%)	P_s (kN)	δ_u (%)	P_u (kN)		
BF	Neg	1.13	43.69	0.51	31.59	3.97	43.72	3.51	7.78
SP-1	Pos	2.68	178.44	0.55	37.32	3.92	166.91	1.49	7.27
SP-2	Pos	2.42	243.61	0.56	89.44	3.43	227.64	1.42	6.16
SP-3	Pos	2.34	189.90	0.49	77.22	3.80	178.06	1.65	7.60

(1) δ_y and P_y at yield point was derived by park method [41]. (2) The failure point was considered to be reached when the strength drops to 85% of the peak strength [42]. (3) The unfavorable one in positive and negative loading direction was considered. (4) the ductility factor was calculated by $\mu_{park} = \delta_u / \delta_y$, $\mu_s = \delta_u / \delta_s$, respectively

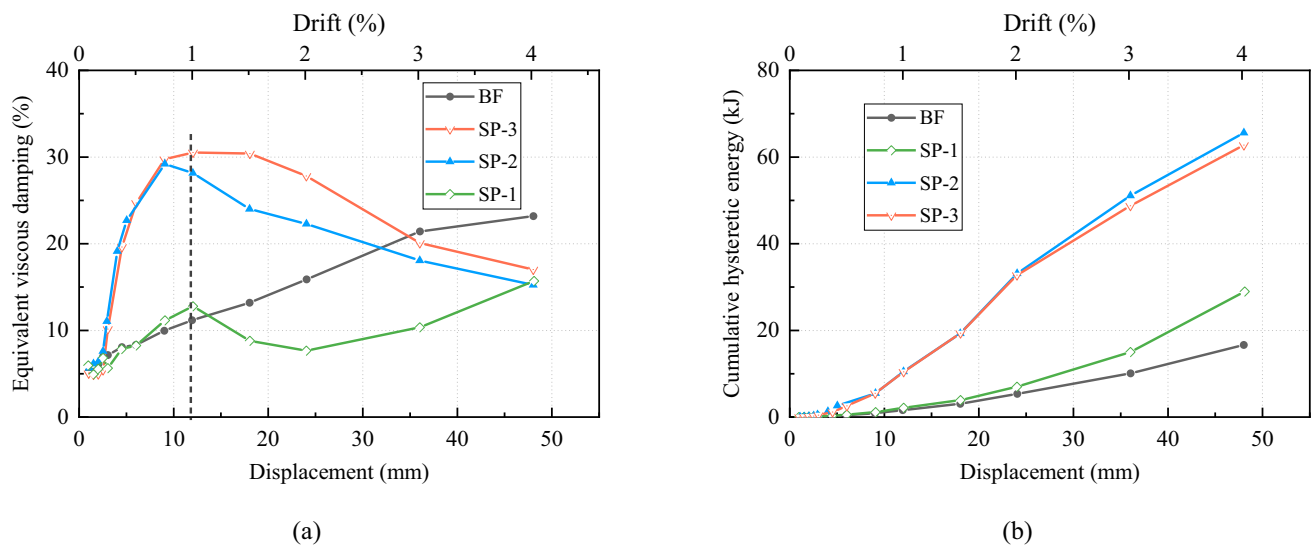


Fig. 20 Comparison of energy dissipation: **a** equivalent viscous damping ratio; **b** cumulative hysteretic energy

the bare frame, thus involves the beam in contributing to energy dissipation and load resistance, which means all of the original structural elements have been fully used.

- The eccentric length of RC beam is an important parameter influencing the ductility capacity and the energy dissipation as well as two-stage extra strength of the frame. Due to the larger eccentricity, the drift capacity of SP-3 increased by 11% (positive direction) than SP-2. Hence, it is suggested that limited eccentricity ratio on account of both ductility and strength requirement should be considered in design.
- Benefit from the low yield point and energy dissipation capacity of mild steel, the retrofitting system can dissipate a large amount of seismic energy in the first stage. Particularly, the equivalent viscous damping ratio of SP-3 has reached over 30% before “compaction”. The limited deformation capacity leads to the failure of the adopted steel coupling beam at a drift ratio of about 3%, which already meet the ultimate displacement ratio (2%) required in the Chinese Code [33]. However, viscous dampers or friction dampers with large deformation capacity could be considered to optimize the retrofitting system to meet higher ductility requirements.
- The work presented herein is a “proof of concept” one and is obviously far from completely understand GESB system. Further studies should include full-scale testing (preferably on more realistic three-dimensional structures) and additional configuration investigations (including brace buckling and damper types), aiming at optimizing further the proposed concept. In addition, the design guide of the system will be proposed in the subsequent studies.

Author contributions JZ methodology, investigation, validation, data curation, visualization, writing—original draft. JS methodology, supervision. HQ conceptualization, supervision.

Declarations

Conflict of interest The authors declare that they have no known competing financial interests or personal relationships that could have appeared to influence the work reported in this paper.

Ethical statement Authors state that the research was conducted according to ethical standards.

References

- Liel AB, Haselton CB, Deierlein GG, Baker JW. Incorporating modeling uncertainties in the assessment of seismic collapse risk of buildings. *Struct Saf.* 2009;31(2):197–211. <https://doi.org/10.1016/j.strusafe.2008.06.002>.
- Ismail N, El-Maaddawy T, Khattak N. Quasi-static in-plane testing of FRCM strengthened non-ductile reinforced concrete frames with masonry infills. *Constr Build Mater.* 2018;186:1286–98. <https://doi.org/10.1016/j.conbuildmat.2018.07.230>.
- Kim Y, Lim SA, Park HS. Optimal seismic retrofit method for reinforced concrete columns with wing walls. *Eng Struct.* 2020. <https://doi.org/10.1016/j.engstruct.2020.110390>.
- Qu Z, Wada A, Motoyui S, Sakata H, Kishiki S. Pin-supported walls for enhancing the seismic performance of building structures. *Earthq Eng Struct Dyn.* 2012;41(14):2075–91. <https://doi.org/10.1002/eqe.2175>.
- Madden GJ, Symans MD, Wongprasert N. Experimental verification of seismic response of building frame with adaptive sliding base-isolation system. *J Struct Eng.* 2002;128(8):1037. [https://doi.org/10.1061/\(ASCE\)0733-9445\(2002\)128:8\(1037\)](https://doi.org/10.1061/(ASCE)0733-9445(2002)128:8(1037)).
- Landi L, Lucchi S, Diotallevi PP. A procedure for the direct determination of the required supplemental damping for the seismic

- retrofit with viscous dampers. *Eng Struct.* 2014;71: 137–49. <https://doi.org/10.1016/j.engstruct.2014.04.025>.
7. Furtado A, Rodrigues H, Varum H, Costa A. Evaluation of different strengthening techniques' efficiency for a soft storey building. *Eur J Environ Civ Eng.* 2017;21(4):371–88. <https://doi.org/10.1080/19648189.2015.1119064>.
 8. Chang S, Chen T, Tran N. Seismic retrofitting of RC columns with RC jackets and wing walls with different structural details. *Earthq Eng Eng Vib.* 2014;2(13):279–92. <https://doi.org/10.1007/s11803-014-0230-4>.
 9. Javadi P, Yamakawa T. Strength and ductility type retrofit of soft-first-story RC frames through the steel-jacketed non-reinforced thick hybrid wall. *Eng Struct.* 2019;186:255–69. <https://doi.org/10.1016/j.engstruct.2019.02.013>.
 10. Boushelham A. State of research on seismic retrofit of RC beam-column joints with externally bonded FRP. *J Compos Constr.* 2010;14(1):49–61. [https://doi.org/10.1061/\(ASCE\)CC.1943-5614.0000049](https://doi.org/10.1061/(ASCE)CC.1943-5614.0000049).
 11. Miano A, Sezen H, Jalayer F, Protá A. Performance-based assessment methodology for retrofit of buildings. *J Struct Eng.* 2019;145(12):15p. [https://doi.org/10.1061/\(ASCE\)ST.1943-541X.0002419](https://doi.org/10.1061/(ASCE)ST.1943-541X.0002419).
 12. Varum H, Teixeira-Dias F, Marques P, Pinto AV, Bhatti AQ. Performance evaluation of retrofit strategies for non-seismically designed RC buildings using steel braces. *Bull Earthq Eng.* 2013;11(4):1129–56. <https://doi.org/10.1007/s10518-012-9421-4>.
 13. Stazi F, Serpilli M, Maracchini G, Pavone A. An experimental and numerical study on CLT panels used as infill shear walls for RC buildings retrofit. *Constr Build Mater.* 2019;211:605–16. <https://doi.org/10.1016/j.conbuildmat.2019.03.196>.
 14. Ahmad N, Masoudi M. Eccentric steel brace retrofit for seismic upgrading of deficient reinforced concrete frames. *Bull Earthq Eng.* 2020;18(6):2807–41. <https://doi.org/10.1007/s10518-020-00808-0>.
 15. Rahimi A, Maheri MR. The effects of steel X-brace retrofitting of RC frames on the seismic performance of frames and their elements. *Eng Struct.* 2020;206: 110149. <https://doi.org/10.1016/j.engstruct.2019.110149>.
 16. TahamouliRoudsari M, Entezari A, Hadidi M, Gandomian O. Experimental assessment of retrofitted RC frames with different steel braces. *Structures.* 2017;11:206–17. <https://doi.org/10.1016/j.istruc.2017.06.003>.
 17. Pan K, Tsai K, Khoo H, Wu A, Li C. Seismic retrofit of reinforced concrete frames using buckling-restrained braces with bearing block load transfer mechanism. *Earthq Eng Struct Dyn.* 2016;45(14):2303–26. <https://doi.org/10.1002/eqe.2763>.
 18. Zahrai SM, Froozanfar M. Improving seismic behavior of MRFs by U-shaped hysteretic damper along diagonal brace. *Int J Steel Struct.* 2019;19(2):543–58. <https://doi.org/10.1007/s13296-018-0139-2>.
 19. Vafaei M, Omar Sheikh AM, Alih SC. Experimental study on the efficiency of tapered strip dampers for the seismic retrofitting of damaged non-ductile RC frames. *Eng Struct.* 2019. <https://doi.org/10.1016/j.engstruct.2019.109601>.
 20. Seong JY, Min KW. An analytical approach for design of a structure equipped with friction dampers. *Proc Eng.* 2011;14:1245–51. <https://doi.org/10.1016/j.proeng.2011.07.156>.
 21. Fateh A, Hejazi F, Jaafar MS, Karim IA, Adnan AB. Design of a variable stiffness bracing system: mathematical modeling, fabrication, and dynamic analysis. *Soil Dyn Earthq Eng.* 2016;80:87–101. <https://doi.org/10.1016/j.soildyn.2015.10.009>.
 22. Zhao J, Qiu H, Sun J, Jiang H. Seismic performance evaluation of different strategies for retrofitting RC frame buildings. *Structures.* 2021;34:2355–66. <https://doi.org/10.1016/j.istruc.2021.09.016>.
 23. Li G, Zhu L, Li H. Displacement-based seismic design for buildings installed hysteretic dampers with hardening post-yielding stiffness. *Adv Struct Eng.* 2019;22(16):3420–34. <https://doi.org/10.1177/1369433219852715>.
 24. Cheraghi A, Zahrai SM. Cyclic testing of multilevel pipe in pipe damper. *J Earthq Eng.* 2017;10(23):1695–718. <https://doi.org/10.1080/13632469.2017.1387191>.
 25. Beigi HA, Christopoulos C, Sullivan T, Calvi M. Seismic response of a case study soft story frame retrofitted using a GIB system. *Earthq Eng Struct D.* 2015;44(7):997–1014. <https://doi.org/10.1002/eqe.2496>.
 26. Tsantilis AV, Triantafyllou TC. Innovative seismic isolation of masonry infills using cellular materials at the interface with the surrounding RC frames. *Eng Struct.* 2018;155:279–97. <https://doi.org/10.1016/j.engstruct.2017.11.025>.
 27. Xu L. Research on mechanical behavior and theoretical model of low-yield-point steel shear panel dampers. Tsinghua University. 2017 (**in Chinese**).
 28. GBJ11-1989. Code for seismic design of buildings. Beijing: China Architecture & Building Press; 1989 (**in Chinese**).
 29. ANSI/AISC 360-10. Specification for structural steel buildings. Chicago: American Institute of Steel Construction; 2010.
 30. Ji X, Hutt CM. Seismic design and application of hybrid coupled walls with replaceable steel coupling beams in high-rise buildings. *Struct Des Tall Spec.* 2020;29(8): e1727. <https://doi.org/10.1002/tal.1727>.
 31. ANSI/AISC 341-10. Seismic provisions for structural steel buildings. Chicago: American Institute of Steel Construction; 2010.
 32. GB 50011-2010. Code for seismic design of buildings. Beijing: China Architecture & Building Press; 2016 (**in Chinese**).
 33. GB 50010-2010. Code for design of concrete structures. Beijing: China Architecture & Building Press; 2015 (**in Chinese**).
 34. Ghobarah A, El-Attar M, Aly NM. Evaluation of retrofit strategies for reinforced concrete columns: a case study. *Eng Struct.* 2000;22(5):490–501. [https://doi.org/10.1016/S0141-0296\(98\)00137-0](https://doi.org/10.1016/S0141-0296(98)00137-0).
 35. GB/T 50081-2002. Standard for test method of mechanical properties on ordinary concrete. Beijing: China Architecture & Building Press; 2003 (**in Chinese**).
 36. GB/T 50152–2012. Standard for test method of concrete structures. Beijing: China Architecture & Building Press, 2012 (**in Chinese**).
 37. GB/T 228.1-2010. Metallic materials-tensile testing-part 1: method of test at room temperature. Beijing: Standards Press of China; 2010 (**in Chinese**).
 38. GB/T 18942.1-2003. Polymeric material, cellular flexible—determination of stress-strain characteristic in compression—part 1: low-density materials. Beijing: Standards Press of China; 2003 (**in Chinese**).
 39. FEMA 461. Interim Testing Protocols for Determining the Seismic Performance Characteristics of Structural and Nonstructural Components. Redwood City, California: Applied Technology Council. 2007.
 40. Ren X. Study on strengthening and seismic performance of reinforced concrete-steel irregular hybrid frame structures. Zhejiang: Zhejiang University; 2018. (**in Chinese**).
 41. FEMA356. Prestandard and commentary for the seismic rehabilitation of building. Washington, D.C.: Federal Emergency Management Agency; 2000.
 42. JGJ/T 101-2015. Specification for seismic test of buildings. Beijing: China Architecture & Building Press; 2015 (**in Chinese**).
 43. Chopra A. Dynamics of structures-theory and applications to earthquake engineering. Englewood Cliffs: Prentice-Hall; 2017.